Classification of brain pericytes based on cell structure, location, and α-smooth muscle actin content

Roger I. Grant[1], David A. Hartmann[1], Robert G. Underly[1], and Andy Y. Shih[1,2]

[1]Department of Neurosciences and [2]Center for Biomedical Imaging, Medical University of South Carolina, Charleston, SC, USA

Abbreviated title: Pericyte heterogeneity in mouse brain

Abstract:	200 words
Narrative:	4900 words
References:	44
Figures:	6 main (all color), 4 supplementary (all color)
Table	1
Video	1 (color)

Abbreviations:

FITC	Fluorescein isothiocyanate
NG2	Neural/glial antigen 2
PDGFRβ	Platelet-derived growth factor receptor β
α-SMA	α-smooth muscle actin
SMC	Smooth muscle cell
EP	Ensheathing pericyte
MP	Mesh pericyte
TSP	Thin-strand pericyte

Funding: Our work is supported by grants to A.Y.S. from the NINDS (NS085402, NS096997), the Dana Foundation, the American Heart Association (14GRNT20480366), South Carolina Clinical and Translational Institute (UL1TR000062), and an Institutional Development Award (IDeA) from the NIGMS under grant number P20GM12345. D.A.H. is supported by awards NIH T32 GM08716, NIH - NCATS (UL1 TR001450 and TL1 TR001451), and NIH-NINDS F30NS096868.

Conflicts of interest: The authors have no financial or non-financial conflicts of interest.

Correspondence: Andy Y. Shih
Department of Neurosciences
Medical University of South Carolina
173 Ashley Ave. CRI 406
Charleston, SC 29425
Office: 843-876-1868
Fax: 843-792-4423
Email: shiha@musc.edu

ABSTRACT

Smooth muscle cells and pericytes, together called mural cells, coordinate numerous vascular functions. Canonically, smooth muscle cells are ring-shaped and cover arterioles with circumferential processes, whereas pericytes extend thin processes that run longitudinally along capillaries. Nearly a century ago, Zimmerman described mural cells with mixed features of smooth muscle cells and pericytes, which he termed "transitional pericytes". Recent studies suggest that transitional pericytes are critically positioned to regulate cerebral blood flow, but there remains considerable confusion on how to identify and categorize them. Here, we use metrics of cell morphology, vascular territory, and α-smooth muscle actin expression to test the hypothesis that transitional pericytes can be distinguished from canonical smooth muscle cells and pericytes. We first imaged fluorescently-labeled mural cells in large volumes of optically-cleared mouse cortex to elucidate the location of potential transitional pericytes. Subsequent investigation of isolated mural cells revealed that one type of transitional pericyte, which we called "ensheathing pericytes", could be reliably distinguished. Ensheathing pericytes possessed protruding ovoid cell bodies and had elongated processes that encircled the vessel lumen. They were rich in α-smooth muscle actin and occupied proximal branches of penetrating arteriole offshoots. We provide guidelines to identify ensheathing pericytes and other mural cell types.

INTRODUCTION

Arteries and arterioles are covered by smooth muscle cells, which are short, ring-shaped and densely packed. In contrast, capillaries are covered by pericytes with intermittent, protruding cell bodies and thin processes that run longitudinally along capillaries.[1] Smooth muscle cells and pericytes lie at opposite ends of a spectrum with regard to appearance and vascular territory. Yet, they form a seamless network that covers the entire vascular bed. Following early description of pericytes by Rouget[2], studies by Zimmermann[3] and Mayer[4] showed that smooth muscle cells and pericytes are bridged by mural cells with hybrid features of both cell types, which were referred to as "transitional pericytes".[5] Zimmermann emphasized the difficulty in studying different pericyte subtypes with methods of his time, which did not allow individual mural cells to be clearly visualized. Today, surveys of pericyte diversity remain challenging because cellular morphology and 3-dimensional organization of blood vessels cannot be gathered from immunostaining of thin tissue sections. Accepted immunohistochemical stains for pericytes, such as PDGFRβ and CD13 (aminopeptidase N)[1, 6], label contiguous groups of mural

cells, precluding the assessment of individual cells. Consequently, transitional pericytes have remained poorly defined and become a source of confusion in the field.

The role of pericytes in cerebral blood flow regulation has been a controversial issue.[7] Some groups have concluded that pericytes regulate cerebral blood flow *in vivo*[8-11], while other groups have refuted this claim[12-14] However, much of this controversy appears to be due to a lack of consensus on how to define a transitional pericyte. For example, most groups have shown that proximal branches of penetrating arterioles are contractile *in vivo*[8, 12, 13], and that the mural cells that cover these vessels appear to fit the concept of transitional pericytes, *i.e.,* protruding cell body like pericytes, and processes encircling the lumen like smooth muscle cells. Yet, these cells are usually bundled together with either canonical smooth muscle cells[13] or pericytes[8] by different research groups, despite their distinct appearance. This inevitably leads to confusion on which mural cells were studied, and the role of one cell type being mistaken for the other. A consensus on how to distinguish mural cell types, as well as the names of different microvascular territories they occupy, would help greatly with the interpretation of studies on cerebral pericytes.

Pericytes are diverse in structure[6] and it is not clear whether transitional pericytes can be isolated as a distinct cell group, or if they exist in a continuum with other pericytes. The goal of this study was therefore to test the hypothesis that transitional pericytes can be distinguished from canonical smooth muscle cells and pericytes, based on cell morphology, α-SMA content, vascular location, or a combination of these metrics. We measured these features from individual mural cell types, and statistically compared them among different mural cell groups. We further examined the relationship between mural cell type and vascular metrics such as lumen diameter and vascular branch order. To overcome past methodological limitations, we imaged intact cerebrovascular networks in optically-cleared tissues to understand the vascular territories occupied by each mural cell type. Further, transgenic mice with sparsely-labeled fluorescent mural cells were used to quantify and compare the morphologies of isolated mural cells.[6] Our approach was able to reliably identify one transitional pericyte type, which past studies have shown is involved in regulation of normal cerebral blood flow.

METHODS

The Institutional Animal Care and Use Committee at the Medical University of South Carolina approved the procedures used in this study. The University has accreditation from the Association for Assessment and Accreditation of Laboratory Animal Care International, and all experiments were performed within its guidelines. All data was analyzed and reported according to ARRIVE guidelines.

Animals. Heterozygous male PDGFRβ-Cre[15] mice, a generous gift from Prof. Volkhard Lindner of the Maine Medical Center Research Institute, or NG2-CreER^{TM} mice (#008538; Jackson labs)[16] were bred with homozygous female Ai14 reporter mice (#007914; Jackson labs)[17] to produce PDGFRβ-tdTomato, and NG2-tdTomato offspring. We used both male and female offspring for all parts of this study. As previously described[6], PDGFRβ-tdTomato mice provided a contiguous label of nearly all mural cells throughout the cerebrovasculature, while NG2-tdtomato provided a sparse labeling of mural cells following induction of Cre recombinase expression using tamoxifen (100mg/kg i.p. dissolved 9:1 corn oil:ethanol for 1 or 2 days).

Tissue fixation. Mice between 3 to 9 months of age were perfusion fixed with phosphate-buffered saline (PBS) containing 10 units/mL heparin, followed by 4% paraformaldehyde (PFA) in PBS through a trans-cardiac route. After perfusion, the brain was extracted and placed in 4% PFA in PBS. Brains were then transferred to PBS with 0.01% sodium azide after overnight post-fixation for longer term storage.

Tissue processing for optically-cleared specimens. Coronal brain slices from PDGFRβ-tdTomato mice were collected at a thickness of 0.5 to 1 mm. Slices were first subjected to an antigen retrieval protocol. This consisted of a 1-hour incubation in a 1:2 ratio of 0.25% trypsin-EDTA (Sigma-Aldrich; T4049) and PBS at 37°C in a water bath. This was followed by 1-hour of washing in PBS at room temperature under slow nutation. Slices were then incubated with a FITC-conjugated α-SMA antibody (Sigma-Aldrich; F3777) for 1-week. The antibody was used at a dilution of 1:200 in an antibody solution composed of 2% Triton X-100 (v/v, Sigma-Aldrich; X100), 10% goat serum (v/v, Vector Laboratories; S1000), and 0.1% sodium azide (w/v, Sigma-Aldrich; S2002) in PBS. Negative control samples for α-SMA staining were incubated at the same time, using adjacent slices from the same animal, in solution without α-SMA antibody (**Supplemental Fig. 2a,b**). This control confirmed that most green fluorescent signal was indeed from detection of α-SMA protein, though autofluorescence was also detected. After 1-week of immunostaining, slices were washed in PBS for 2-hours. We then cleared the tissues using the "See Deep Brain" (SeeDB) method over 4 days [18]. On the fifth day, slices were imaged with two-photon microscopy while immersed in full SeeDB solution. All incubations were performed at room temperature under slow nutation, with samples protected from light with aluminum foil.

Tissue processing for thin sections. Brain slices from NG2-tdTomato mice were collected at thickness of 100 to 200 μm. Slices underwent the same antigen retrieval protocol mentioned above (1-hour trypsin treatment), then were incubated overnight in antibody solution with the following additions: α-SMA primary antibody from mouse host (1:200 dilution; Sigma-Aldrich; A5228) and FITC-conjugated tomato lectin (1:250 dilution; Vector Labs; FL-1171). Following overnight incubation, we washed slices in PBS for 30 minutes, and then transferred to antibody solution containing anti-mouse Alexa 647

secondary antibody (1:500 dilution; ThermoFisher; A31626) for a 2-hour incubation period. Slices were then washed again in PBS for 30 minutes, mounted onto glass slides, and sealed with Fluoromount G (Southern Biotech; 0100-01) under a coverslip. To ensure endogenous mouse IgGs did not interfere with detection of α-SMA, we also examined a rabbit polyclonal α-SMA antibody (1:200; Abcam; ab32575), and found similar patterns of staining compared to the α-SMA antibody from mouse host (**Supplementary Fig. 2c**).

Two-photon imaging of optically-cleared specimens. Imaging was performed with a Sutter Moveable Objective Microscope and a Coherent Ultra II Ti:Sapphire laser source. Cleared tissues were mounted in a small petri dish immersed in SeeDB solution, then covered with a 100 μm thick glass coverslip. Imaging was performed at 975 nm excitation under a 20-X, 1.0 NA water-immersion objective (XLUMPLFLN; Olympus). Green and red fluorescence emission was collected through 515/30 (Chroma ET605/70m-2P) and 615/60 (Chroma ET510/50m-2P) filters, respectively. Image stacks were collected in the barrel field of the primary somatosensory cortex, located by comparing brain regions with a mouse atlas.[19] We imaged penetrating arterioles with branches that were contained within the tissue slice. Two to three image stacks were collected to capture the entirety of a penetrating arteriole, often spanning the pial surface to the callosum. Imaging resolution was 0.63 μm per pixel in the lateral plane (medial-lateral axis) and a z-step of 1 μm was used (anterior-posterior axis). Laser powers at 975 nm were 25 mW at the sample surface, and 220 mW at ~400 um in depth. Image volumes were stitched using XuvTools [20] and viewed in Imaris software (Bitplane).

Confocal imaging of thin sections. Imaging was performed on a Leica TCS SP2 AOBS Confocal Microscope (Leica Microsystems, Inc.) using 20-X (HC PlanAPO 20x/0.7 CS), 40-X (HCX PlanAPO CS 40x/1.25-0.75 Oil immersion), or 63-X(HCX PlanAPO CS 63x/1.4-0.6 Oil immersion) objectives, which respectively had lateral resolution of 0.73, 0.37, and 0.23 μm per pixel. Step sizes in the z-dimension were either 0.5 or 1 μm. Continuous wave lasers with 488, 543, and 633 nm excitation wavelengths were used for FITC, tdTomato, and Alex647, respectively. Emission was collected through a prism spectrophotometer utilizing an acousto-optical tuning filter to collect all channels simultaneously. Images were collected at 1024x1024 pixel size, using line scan averaging of 4, and were viewed and analyzed in FIJI software.

Analysis of two-photon imaging datasets. In total, we examined 52 offshoots extending from 7 penetrating arterioles, collected over 2 mice. Each penetrating arteriole offshoot emerged as a single vessel from the 0th order penetrating arteriole. As this 1st order branch ramified into the capillary bed, we followed each possible route with new bifurcations and recorded the observation of ovoid cell bodies, α-SMA termini, and shifts in pericyte coverage. The location of each of these features reported

in **Figs. 2 and 3** was the branch order resulting from averaging over all vascular routes for each penetrating arteriole offshoot. Ovoid cell bodies were "bump on a log" somata that protruded from the wall of the vessel, a key feature of pericytes. The α-SMA termini were identified visually as abrupt reductions of α-SMA-FITC fluorescence. Shifts in pericyte coverage were defined as locations where coverage in the tdTomato channel changed from completely ensheathing or mesh-like to thin strands running longitudinally along the vessel.

Analysis of confocal imaging datasets. We targeted data collection to four mural cell groups, decided *a priori* based on data obtained from optically-cleared specimens: (1) Smooth muscle cells, found on 0th order penetrating arterioles with short, ring-like morphology, (2) ensheathing pericytes on proximal branches of penetrating arteriole offshoots, which completely covered the endothelium, and exhibited α-SMA staining, (3) mesh pericytes deeper in the capillary bed, which partially covered the endothelium and did not have α-SMA staining, and (4) thin-strand pericytes deeper in the capillary bed that possessed long, thin processes and did not have α-SMA staining. All pericyte subtypes had a clear protruding ovoid cell body, while smooth muscle cells did not. We analyzed 2-D, average-projected confocal images of individual cells. Care was taken to only analyze isolated cells that were fully contained within the image stack. All analyses were performed in FIJI software. The intensity of α-SMA staining (Alexa 647) was measured by averaging pixel values from the far red channel within a mask of the cell generated in the tdTomato channel (**Fig. 4g**). Cell length was the combined length of vasculature contacted by either the cell body or processes, measured using the 'Segmented Line' tool in FIJI (**Fig. 5a-d,i**). Vessel diameter was measured by drawing a line across the vessel width at the location of the tdTomato-positive cell body, if present, in the channel containing FITC-lectin (**Fig. 5a-d,l & Supplementary Fig. 3**). Some vessels with a noticeable diameter gradient were measured at either end of the cell body and then averaged for better accuracy. Coverage measurements were ascertained by visually thresholding average-projected tdTomato images, taking care to ensure all cellular processes were captured in the thresholded image. This roughly equated to a threshold set at one standard deviation below each cells mean intensity value. We then demarcated the area of vessel contacted by each pericyte in the FITC-lectin channel. The area labeled with tdTomato was then divided by the vessel area to provide a measure of coverage (**Fig. 5e-h,j**).

Statistics. Pearson's correlation tests for data from optically-cleared specimens were performed in MatLab for data. Analyses of confocal data was done with SPSS (SPSS Statistics 24, IBM). Statistical tests used for various comparisons are stated in the corresponding figure legend. Welch's one-way ANOVA with Games-Howell *post-hoc* test was used for data sets that passed a Lilliefors test of normality. To adjust for multiple comparisons, the p-value for significance (0.05) was divided by the

total number of comparisons for 4 mural cell groups (6 comparisons). Kruskall-Wallis test with Dunn-Bonferroni *post-hoc* test was used for data sets that did not pass the test for normality.

RESULTS

The mural cell continuum visualized in optically-cleared tissues.

To visualize murals cells and α-SMA expression within a preserved microvascular network in PDGFRβ-tdTomato mice, we immunostained and then optically cleared 0.5 to 1 mm thick coronal brain slices containing the primary barrel field of the somatosensory cortex. We collected high-resolution images using two-photon microscopy, and stitched adjacent image volumes to produce large data sets that followed penetrating arterioles and their offshoots as they descend from the pial surface to the corpus callosum (**Fig. 1a-c, Supplementary video 1**). Our studies focused on cortical penetrating arterioles and their offshoots because most *in vivo* two-photon imaging studies of cerebral blood flow regulation have focused on this vessel type.[8, 13, 21]

Definitions.

It is essential to first explain how we chose to define microvessel types and their organization. In line with previous studies of vascular topology[8, 13], we referred to the main penetrating arteriole trunk as the 0th branch order (**Fig. 1d**; right side). The first segment of an offshoot was called the 1st order branch. Each subsequent bifurcation encountered, regardless of branch size, then increased branch order by 1. This branch ordering system, however, does not apply to the base of the penetrating arteriole, where the 0th order vessel tapers and splits into multiple branches and it becomes difficult to define the 0th order vessel (**Supplementary Fig. 1**).

In addition, we used the term "pre-capillary arteriole" for any branch 1st order or greater with α-SMA staining (**Fig. 1d**; left side). Microvessels that do not express α-SMA, and are not ascending venules, were called capillaries. Mural cells residing on both pre-capillary arterioles and capillaries, including transitional phenotypes, were referred to as pericytes, because we found that the vast majority possessed protruding ovoid cell bodies (*i.e.,* "bump on a log"), a classic feature of the pericyte. This is also in accordance with studies by Zimmermann[3] and others.[1, 22]

Minimal variation in pericyte transitions with cortical depth.

We examined 52 penetrating arteriole offshoots and their associated downstream branches (collected over 7 penetrating arterioles from 2 mice). For each offshoot, we followed all daughter branches and recorded the branch orders at which the following first emerged: (1) a protruding ovoid cell body (**Fig. 2a**; arrowhead), (2) an abrupt cutoff in α-SMA staining, called a "terminus" (**Fig. 2b**; arrow), and (3) a

shift in pericyte coverage, a measure of where pericyte processes that ensheathed the vessel transitioned to string-like processes (**Fig. 2c**; arrowhead). We report the average branch order of the occurrence of these pericyte features for each offshoot examined.

We found that ovoid cell bodies emerged on 1st order branches for nearly all offshoots examined (**Fig. 2d**); ~10% occurred on 2nd order branches, but were on or immediately after the bifurcation. The α-SMA termini were found over 0th to 4th order branches (**Fig. 2e**), with 1st and 2nd order being the most common locations. In this case, 0th order termini referred to branches where α-SMA expression never extended beyond the penetrating arteriole trunk. Finally, shift in pericyte coverage was observed over a broad range of branch orders, from 1st to 7th (**Fig. 2f**). While there was higher variance for location of α-SMA termini and shift in pericyte coverage, the average branch order of all three features was relatively uniform over different cortical depths (**Fig. 2g-i**). For shift in pericyte coverage, a shallow peak was observed at ~400 μm in cortical depth, which roughly corresponds to layer 4 in cortex (**Fig. 2i**).[23]

α-Smooth muscle actin and pericyte coverage extends farther with larger branches.

We noticed that penetrating arteriole offshoots with small diameter often had no detectable α-SMA (**Fig. 3a**), while branches with larger diameters supported α-SMA expression up to 4 branch orders downstream (**Fig. 3b**). We therefore asked how pericyte cell bodies, α-SMA termini and pericyte coverage related to the size of the offshoot. To obtain a metric for offshoot size, we quantified the diameter of the 1st order branch for each offshoot (**Fig. 3a,b**; distance between arrowheads). While no correlation was found between location of first ovoid cell bodies and branch diameter (**Fig. 3c**), the locations of both α-SMA termini and coverage shifts were strongly correlated with 1st order branch diameter (**Fig. 3d,e**). Thus, a step-wise transition of pericyte features could be clearly observed on larger penetrating arteriole offshoots:

Pericyte cell bodies emerge (~1st order) → α-SMA expression terminates (~2rd order) → shift in vessel coverage (~4th order).

Heterogeneity of pericyte characteristics.

We suspected that the step-wise transition of pericyte features in PDGFRβ-tdTomato mice reflected the presence of transitional pericytes. To test this possibility, we examined in detail the characteristics of isolated pericytes in sparsely-labeled NG2-tdTomato mice (**Fig. 4a,b**)[6]. While all pericytes sampled possessed ovoid cell bodies, in accordance with the definitions above, the processes extending from pericyte cell bodies and their degree of vessel coverage were highly varied (**Fig. 4d-f**, see tdTomato channel), compared to the more uniform ring-like smooth muscle cells (**Fig. 4c**). To facilitate the testing of our hypothesis that transitional pericyte types could be quantitatively distinguished from other mural

cells, we provided names for three apparent pericyte types, based upon the appearance of their processes: ensheathing, mesh and thin-strand, building upon our past descriptions.[6] In the following sections, we obtain metrics of α-SMA expression, vascular territory (branch order and vessel diameter), and/or cellular morphology for comparison between each pericyte type and smooth muscle cells.

α-Smooth muscle actin expression between pericytes types.

We first compared the intensity of α-SMA immunofluorescence between mural cells (**Fig. 4d-f**, see α-SMA channel), which reflects α-SMA protein content. The level of α-SMA in ensheathing pericytes was comparable to smooth muscle cells, and was significantly higher than both mesh and thin-strand pericytes (**Fig. 4g**). In a past study, we observed faint levels of α-SMA in mesh pericytes.[6] However, a more detailed analysis in the current study showed that α-SMA immunofluorescence in mesh pericytes and thin-strand pericytes were both no higher than background. Thus, α-SMA expression can distinguish ensheathing pericytes from mesh and thin-strand pericytes.

Vascular territory of pericytes types.

In NG2-tdTomato mice, ensheathing pericytes were found on an average branch order of 1.4 ± 0.2, mesh pericytes on 3.7 ± 0.7, and thin-strand pericytes on 5.7 ± 0.4. The branch order of ensheathing pericytes was statistically lower than thin-strand pericytes (*$p<0.001$; Kruskal Wallis and Dunn-Bonferroni *post hoc*), but not mesh pericytes ($p=0.42$). Mesh and thin-strand could not be distinguished based on branch order ($p=1.00$). Ensheathing pericytes were also found on larger diameter microvessels than thin-strand pericytes, but not mesh pericytes. Vessel diameters between mesh and thin-strand pericytes were not different (**Supplementary Fig. 3b**).

Morphological features of pericyte types.

We next asked if mural cells could be statistically separated based on cell morphology. We examined cell length, where pericyte length was calculated as the total length of pericyte soma and processes in contact with FITC-lectin-labeled capillary (**Fig. 5a-d**; gray lines). As expected, smooth muscle cells on the 0th order penetrating arterioles were short in length, averaging only ~20 μm. The length of each pericyte type, however, was progressively greater than the smooth muscle cell with ensheathing, mesh and thin-strand pericytes extending over ~40, 100, and 150 μm of capillary, respectively (**Fig 5i**). Ensheathing pericytes were statistically shorter in length than both mesh and thin-strand pericytes. Mesh and thin-strand pericytes, however, were not different in length from each other. Interestingly, mural cell length increased exponentially as vessel diameter decreased (**Supplementary Fig. 3a**).

As a test of self-consistency for the cell length data, we returned to data from PDGFRβ-tdTomato mice to measure the inter-somal distance of pericytes at locations relevant to ensheathing pericytes and mesh/thin-strand pericytes, *i.e.*, upstream and downstream of the α-SMA terminus (**Supplementary Fig. 4**). Individual pericyte morphologies could not be discerned in these mice, so we collectively referred to mesh and thin-strand pericytes as capillary pericytes. Since the processes of neighboring pericytes do not overlap [13], we reasoned that inter-somal distance should also relate to cell length. Indeed, the inter-somal distance of ensheathing pericytes was significantly shorter compared to mesh or thin-strand pericytes.

Finally, we examined the extent of vessel coverage offered by each pericyte type. Coverage was calculated from average projected images as the percentage of tdTomato labeled area (**Fig. 5e-h**; red) divided by a larger area demarcated by lectin-labeled endothelium (**Fig. 5e-h**; black). Vessel coverage by ensheathing pericytes (>95%) was significantly higher than both mesh pericytes (65%) and thin-strand pericytes (50%)(**Fig. 5j**). The modest difference in coverage between mesh and thin-strand pericyte was found to be statistically significant (**Fig. 5j**).

DISCUSSION

Using quantitative analyses of mural cell histology, we found evidence to support our hypothesis that transitional pericytes can be statistically distinguished from canonical smooth muscle cells and pericytes. We initially identified two pericytes types, ensheathing and mesh pericytes, that exhibited features of both smooth muscle cells (encircling of the lumen) and pericytes (protruding ovoid cell body and elongated processes). However, detailed comparisons revealed that only ensheathing pericytes could be separated from smooth muscle cells (based on branch order and cell morphology), and from mesh and thin-strand pericytes (based on α-SMA content, cell length, and vessel coverage). In contrast, mesh pericytes could not be separated from thin-strand pericytes. Although modest differences were found in vessel coverage (**Fig. 5j**), mesh and thin strand pericytes both lacked α-SMA staining, and heavily overlapped in vascular territories and cell length. This suggests that mesh and thin-strand pericytes exist within a continuum, and should be considered as one group, termed "capillary pericytes".

What is an ensheathing pericyte and a capillary pericyte? These new data allow us to provide clearer definitions for the different pericyte types that adorn brain microvessels (**Fig. 6a**). We conclude that ensheathing pericytes are an unambiguously identifiable "transitional pericyte", and we suggest that the term ensheathing pericyte should be used to describe these cells to avoid confusion with mesh pericytes that appear morphologically similar, but are α-SMA-negative. Ensheathing pericytes occupy

pre-capillary arterioles and are α-SMA-positive. They cover the vessel nearly 100%, but differ from smooth muscle cells because they possess an ovoid cell body, and are more elongated. In contrast, capillary pericytes, comprised of mesh and thin-strand pericytes, are α-SMA-negative, longer in total cell length, and bear processes of varying complexity that only partially cover the vessel, *i.e.*, 40-80%. Capillary pericytes occupy the capillaries, defined as microvessels after the α-SMA terminus. To further facilitate the classification of mural cells, we provide a flow chart (**Fig. 6b**) that relies only on knowledge of vascular topology and α-SMA expression. We anticipate that this flow chart and nomenclature will improve clarity in future discussions of cerebral pericytes in normal and pathophysiological brain states. Oftentimes there is insufficient information in studies to determine if results apply to ensheathing pericytes, capillary pericytes, or both, which likely have different contributions to blood flow regulation

Identifying ensheathing pericytes in vivo. *In vivo* imaging studies seeking to differentiate between ensheathing and capillary pericytes would benefit from an α-SMA label, such as that provided by the SMA-mCherry mouse line used by Hill *et al.*[13] Our data also suggest, however, that ensheathing pericytes reside only between 1st to 4th order branches. This information may be useful for conditions in which information on α-SMA expression is not attainable. For example, targeting branches beyond 4th order ensures one is targeting capillary pericytes, while targeting branches under 4th order, on large penetrating arteriole offshoots, increases the likelihood of studying ensheathing pericytes, but does not guarantee it.

Microvessel diameter and pericyte type. Ensheathing pericytes tended to occupy microvessels that were 3-4 μm larger (~140%) than capillary pericytes. Yet, these differences were small in absolute magnitude and the diameters overlapped greatly between groups (**Supplementary Fig. 3b**). Further, when interpreting the study by Hill *et al.*[13] using the mural cell classification presented here, it appears that the basal tone applied by ensheathing pericytes *in vivo* can make the diameter of pre-capillary arterioles indistinguishable, and sometimes even smaller than nearby capillaries. Pre-capillary arteriole and capillary diameter can further change with the anesthetic state of the animal.[24] For these reasons, microvessel diameter alone is unlikely to be a reliable means to differentiate between ensheathing and capillary pericytes.

Are ensheathing pericytes contractile in vivo? To date, five major studies have examined the role of pericytes in regulating blood flow in the intact brains of live mice. These *in vivo* studies appeared to report opposing results, with Hall *et al.* [8] and Kisler *et al.* [10] suggesting a role for pericytes in physiological blood flow regulation, while Hill *et al.* [13], Fernandez-Klett *et al.* [12], and Wei *et al.* [14] suggested the contrary. Upon closer inspection, however, it becomes evident that there is consistency

in the finding that capillary branches close to penetrating arterioles, *i.e.* 1st-4th order branches, occupied by ensheathing pericytes, exhibit lumen diameter change during normal brain activity. Hill *et al.* further reported ischemia-reperfusion induced vasoconstriction at the same proximal branches, but not with vessels deeper in the capillary bed.[13] Similarly, Fernandez-Klett *et al.* showed vasoactivity at proximal branches with bicuculline-induced neuronal activation and spreading depression.[25] Thus, the idea that ensheathing pericytes possess contractile function is consistent between multiple groups that have studied vasoreactivity *in vivo*.

Are capillary pericytes contractile in vivo? While it is challenging to assess vascular topology in acute brain slices, past studies have shown that about 50 to 70% of pericytes stimulated by agonist cause local capillary diameter change.[8, 26] This suggests that a greater proportion of pericytes than just ensheathing pericyte possess contractile function. Interestingly, optogenetic stimulation of capillary pericytes in the study by Hill *et al*. did not yield any perceptible change in capillary diameter.[13] Yet, cells with capillary pericyte morphology contract locally during *in vivo* application of U46619, a TBXA2 receptor agonist and potent vasoconstrictor[25], though not in response to local neural activity. Studies of capillary diameter during ischemia also indicate reduced capillary constriction that may be due to pericyte contraction.[9, 27-29] Further, unpublished studies from our group[30] suggest that capillary pericytes can alter capillary diameter and red blood cell flow *in vivo* with stronger optogenetic depolarization than that used by Hill *et al*. [13] Thus, there is mounting evidence that depolarization of capillary pericytes in pathological scenarios such as stroke may lead to sustained capillary constriction, such as with pericyte "rigor" described by Hall *et al.*[8] Actin isoforms other than α-SMA, *i.e.,* smooth muscle γ-actin, are reportedly expressed in pericytes[31], and may be involved in this mode of pericyte contraction.[32]

Limitations and future steps. Our study focused on the arteriole pole of microvasculature due to its relevance in neurovascular coupling. However, cells with transitional features also exist on post-capillary venules, and these cells may be involved in regulation of immune cell entry [33]. We suspect that the approach used here will not provide clear classifications for venular pericytes, since α-SMA expression is generally lower and less clear-cut in venules.[1] It is also unclear how our approach to categorize mural cells in mouse cortex translate to vasculature of other brain regions. Further, similar gradients in α-SMA expression and vessel coverage has been reported in other organs[34, 35], but pericyte density, morphology and vascular topology may differ greatly from brain[36]. Finally, it is important to note that pericytes are more diverse than the classification provided here, with roles in blood-brain barrier integrity [37-39] and blood-brain barrier degradation during pathology [40, 41], immune cell entry [33], new vessel formation [42], and potentially, the production of pluripotent stem cells [22]. The powerful genetic and biochemical approaches recently used to dissect pericyte genetics[43, 44] should be

related to pericyte morphology and vascular location. This will help to link pericyte expression profiles with functional roles revealed by *in vivo* studies

Acknowledgements. We thank Catherine Hall, Mark T. Nelson, and Pablo Blinder for helpful discussion. We also thank Andrée-Anne Berthiaume, Ashley Watson, and Manuel Levy for critical reading of the manuscript.

Author Contribution Statement. R.I.G., D.A.H., and A.Y.S. designed, executed and analyzed the studies. R.I.G. and D.A.H. wrote the manuscript with feedback from R.G.U. and A.Y.S.

FIGURE LEGENDS

Figure 1. Mural cell organization and vascular structure revealed in optically-cleared mouse cortex. (**a**) Reconstructed volume from barrel cortex of a PDGFRb-tdTomato mouse, showing tdTomato fluorescence. (**b**) The same tissues were immunolabeled with FITC-conjugated α-SMA antibody. (**c**) Composite image of tdTomato and FITC channels. (**d**) Schematic showing the terms used to describe various portions of the vascular anatomy (left side) and the system for ordering microvessel branches as they ramified from the penetrating arteriole.

Figure 2. Minimal variation of pericyte features with penetrating arteriole offshoots at different cortical depths. (**a**) The first observation of an ovoid cell body (arrowhead). The numbers denote branch order, as defined in Figure 1d. (**b**) Examples of α-SMA termini, where α-SMA labeling decreases sharply (arrows). (**c**) Example of a coverage shift (arrowhead), where complete to near complete vessel coverage shifts to thin, longitudinal running processes. (**d-f**) Histograms showing the frequency at which each mural cell feature occurs at each branch order. (**g-i**) Scatterplots of each mural cell feature, showing branch order of occurrence as a function of cortical depth. Running average (window size 200 μm; step size 50 μm) +/- SEM is shown.

Figure 3. α-SMA content and pericyte coverage extend further along larger penetrating arteriole offshoots. First order branches of penetrating arteriole offshoots range in diameter. Examples of small (**a**) and large (**b**) Branches, with diameters of 8 μm and 16 μm at their points of emergence, respectively. Note that α-SMA does not extend into the small branch, while the large branch supports α-SMA for several branch orders. (**c-e**) Scatterplots of each mural cell feature, showing average branch order of occurrence as a function of the 1st order branch diameter. Analysis was performed with Pearson's correlation; n = 52 penetrating arteriole offshoots, collected over 7 penetrating arterioles from 2 mice.

Figure 4. α-SMA content of mural cell types in sparsely labeled NG2-tdTomato mice. (**a**) Wide field view of penetrating arteriole in barrel cortex of NG2-tdTomato mouse. Mural cells are labeled with tdTomato (red) and vascular endothelium was labeled with FITC-conjugated lectin (green). Images were captured from 100 to 200 μm thick coronal brain sections using confocal microscopy. (**b**) The same region of tissue showing immunolabel with α-SMA antibody. (**c**) A smooth muscle cell (SMC) observed on the 0th order penetrating arteriole. Co-label with α-SMA antibody and FITC-lectin is also shown. (**d**) A representative ensheathing pericytes (EP) on a pre-capillary arteriole. (**e**) A representative mesh pericyte (MP) on a capillary. Note that the cell abuts the α-SMA terminus. (**f**) A typical thin-strand pericyte (TSP), *i.e.*, the canonical form of pericyte, on a capillary. (**g**) Intensity of α-SMA exhibited for each mural cell groups. **$p<0.01$, Kruskal-Wallis H test with Dunn-Bonferroni *post-hoc* test; n = 10, 10, 8, and 9 for SMC, EP, MP, and TSP, respectively. Data was collected over 3 mice. Data shown as mean ± SEM.

Figure 5. Mural cell types exhibit varying cell lengths and degrees of vessel coverage. (**a-d**) Examples of each mural cell type, with lines to measure total cell length (gray lines) and vessel diameter (white lines). The length of the thin-strand pericyte extends beyond the image. (**e-h**) Vessel coverage for each mural cell was calculated by dividing tdTomato-positive area (red region) by a mask of the vessel area underlying the cell (black region). (**i,j**) Total cell length and vessel coverage for each mural cell group. **$p<0.01$, ***$p<0.001$, Welch's one-way ANOVA with Games-Howell *post-hoc* test; n = 16, 20, 7, and 19 for SMC, EP, MP, and TSP, respectively. Data was collected over 3 mice. Data shown as mean ± SEM.

Figure 6. Mural cell organization in mouse cortical vasculature and flow chart for classification. (**a**) Schematic showing transition of mural cells as penetrating arteriole offshoots transition from pre-capillary arterioles to capillaries. The names of mural cell groups, features examined in this study, and approximate branch orders of occurrence are depicted. (**b**) Flowchart for distinguishing three major mural cells groups, smooth muscle cells, ensheathing pericytes, and capillary pericytes, in the vasculature of mouse cortex.

Table 1. Metrics measured for pericyte subtypes.

	Cell length (μm)	Vessel diameter (μm)	Vessel Coverage (%)	N (cells)	α-SMA intensity (a.u.)	N (cells)
Smooth muscle cell	17.4 ± 1.5	16.3 ± 1.6	94.8 ± 1.0	16	29.0 ± 9.2	7
Ensheathing pericyte	40.6 ± 2.6	9.3 ± 0.4	94.8 ± 0.9	20	27.4 ± 8.66	10
Mesh pericyte	109 ± 12.2	6.4 ± 0.4	66.6 ± 4.1	7	-1.38 ± 0.49	8
Thin-strand pericyte	149 ± 10.8	5.0 ± 0.1	51.6 ± 1.3	19	0.46 ± 0.15	9

Statistics are provided in figure legends for cell length (Fig. 5i), vessel diameter (Fig. 3b), vessel coverage (Fig. 5j), and α-SMA intensity (Fig 4g).

LITERATURE CITED

1. Armulik A, Genove G, Betsholtz C. Pericytes: Developmental, physiological, and pathological perspectives, problems and promises. *Developmental Cell* 2011; 21(2)**:** 193-215.

2. Rouget C. Memoire sur le developpement la structure et les proprietes physiologiques des capillaires sanguins et lymphatiques. *Arch Physiol Norm Path* 1873; 5**:** 603–663.

3. Zimmermann KW. Der feinere Bau der Blutkapillaren. *Z Anat Entwicklungsgesch* 1923; 68**:** 29-109.

4. Mayer S. Die Muscularisierung der capillaren Blutgefäβe. *Anat Anz* 1902; 21**:** 442-455.

5. Krueger M, Bechmann I. CNS pericytes: concepts, misconceptions, and a way out. *Glia* 2010; 58(1)**:** 1-10.

6. Hartmann DA, Underly RG, Grant RI, Watson AN, Lindner V, Shih AY. Pericyte structure and distribution in the cerebral cortex revealed by high-resolution imaging of transgenic mice. *Neurophotonics* 2015**:** 041402.

7. Attwell D, Mishra A, Hall CN, O'Farrell FM, Dalkara T. What is a pericyte? *Journal of Cerebral Blood Flow & Metabolism* 2015; 36(2)**:** 451-455.

8. Hall CN, Reynell C, Gesslein B, Hamilton NB, Mishra A, Sutherland BA *et al.* Capillary pericytes regulate cerebral blood flow in health and disease. *Nature* 2014; 508(7494)**:** 55-60.

9. Yemisci M, Gursoy-Ozdemir Y, Vural A, Can A, Topalkara K, Dalkara T. Pericyte contraction induced by oxidative-nitrative stress impairs capillary reflow despite successful opening of an occluded cerebral artery. *Nature Medicine* 2009; 15**:** 1031–1037.

10. Kisler K, Nelson AR, Rege SV, Ramanathan A, Wang Y, Ahuja A *et al.* Pericyte degeneration leads to neurovascular uncoupling and limits oxygen supply to brain. *Nature Neuroscience* 2017; Epub ahead of print.

11. Mishra A, Reynolds JP, Chen Y, Gourine AV, Rusakov DA, Attwell D. Astrocytes mediate neurovascular signaling to capillary pericytes but not to arterioles. *Nature Neuroscience* 2016; 19(12)**:** 1619-1627.

12. Fernández-Klett F, Offenhauser N, Dirnagl U, Priller J, Lindauer U. Pericytes in capillaries are contractile *in vivo*, but arterioles mediate functional hyperemia in the mouse brain. *Proceedings of the National Academy of Sciences USA* 2010; 107**:** 22290-22295.

13. Hill RA, Tong L, Yuan P, Murikinati S, Gupta S, Grutzendler J. Regional Blood Flow in the Normal and Ischemic Brain Is Controlled by Arteriolar Smooth Muscle Cell Contractility and Not by Capillary Pericytes. *Neuron* 2015; 87(1)**:** 95-110.

14. Wei HS, Kang H, Rasheed IY, Zhou S, Lou N, Gershteyn A *et al.* Erythrocytes Are Oxygen-Sensing Regulators of the Cerebral Microcirculation. *Neuron* 2016; 91(4)**:** 851-862.

15. Cuttler AS, LeClair RJ, Stohn JP, Wang Q, Sorenson CM, Liaw L *et al.* Characterization of Pdgfrb-Cre transgenic mice reveals reduction of ROSA26 reporter activity in remodeling arteries. *Genesis* 2011; 49(8)**:** 673-680.

16. Zhu X, Hill RA, Dietrich D, Komitova M, Suzuki R, Nishiyama A. Age-dependent fate and lineage restriction of single NG2 cells. *Development* 2011; 138(4)**:** 745-753.

17. Madisen L, Zwingman TA, Sunkin SM, Oh SW, A. ZH, Gu H *et al.* A robust and high-throughput Cre reporting and characterization system for the whole mouse brain. *Nature Neuroscience* 2010; 13**:** 133-140.

18. Ke MT, Fujimoto S, Imai T. SeeDB: a simple and morphology-preserving optical clearing agent for neuronal circuit reconstruction. *Nature Neuroscience* 2013; 16(8)**:** 1154-1161.

19. Franklin KBJ, Paxinos G. *The mouse brain in stereotaxic coordinates*, Third edn Elsevier: New York, New York, 2008.

20. Emmenlauer M, Ronneberger O, Ponti A, Schwarb P, Griffa A, Filippi A *et al.* XuvTools: free, fast and reliable stitching of large 3D datasets. *Journal of Microscopy* 2009; 233(1)**:** 42-60.

21. Tian P, Teng I, May LD, Kurz R, Lu K, Scadeng M *et al.* Cortical depth-specific microvascular dilation underlies laminar differences in blood oxygenation level-dependendent functional MRI signal. *Proceedings of the National Academy of Sciences USA* 2010; 107(34)**:** 15246-15251.

22. Dore-Duffy P. Pericytes: Pluripotent Cells of the Blood Brain Barrier. *Current Pharmaceutical Design* 2008; 14**:** 1581-1593.

23. Blinder P, Tsai PS, Kaufhold JP, Knutsen PM, Suhl H, Kleinfeld D. The murine cortical angiome: An interconnected vascular network with noncolumnar patterns of blood flow. *Nature Neuroscience* 2013; 16**:** 889-897.

24. Cudmore RH, Dougherty SE, Linden DJ. Cerebral vascular structure in the motor cortex of adult mice is stable and is not altered by voluntary exercise. *Journal of Cerebral Blood Flow & Metabolism* 2016; Epub ahead of print.

25. Fernández-Klett F, Offenhauser N, Dirnagl U, Priller J, Lindauer U. Pericytes in capillaries are contractile in vivo, but arterioles mediate functional hyperemia in the mouse brain. *Proceedings of the National Academy of Sciences* 2010; 107(51)**:** 22290-22295.

26. Peppiatt CM, Howarth C, Mobbs P, Attwell D. Bidirectional control of CNS capillary diameter by pericytes. *Nature* 2006; 443**:** 642-643.

27. Taylor ZJ, Hui ES, Watson AN, Nie X, Deardorff RL, Jensen JH *et al.* Microvascular basis for growth of small infarcts following occlusion of single penetrating arterioles in mouse cortex. *Journal of Cerebral Blood Flow & Metabolism* 2016; 36(8)**:** 1357-1373.

28. Morris DC, Davies K, Zhang Z, Chopp M. Measurement of cerebral microvessel diameters after embolic stroke in rat using quantitative laser scanning confocal microscopy. *Brain Research* 2000; 876**:** 31-36.

29. Garcia JH, Liu K-F, Yoshida Y, Chen S, Lian J. Brain Microvessels: Factors altering their patency after the occlusion of a middle cerebral artery (Wistar rat). *American Journal of Pathology* 1994**:** 728-740.

30. Hartmann DA, Grant RI, Shih AY. Probing the contractility of capillary pericytes in vivo with optogenetics. *Society for Neuroscience Abstract #319.01* 2016.

31. DeNofrio D, Hoock TC, Herman IM. Functional sorting of actin isoforms in microvascular pericytes. *The journal of cell biology* 1989; 109(1)**:** 191-202.

32. Kim HR, Gallant C, Leavis PC, Gunst SJ, Morgan KG. Cytoskeletal remodeling in differentiated vascular smooth muscle is actin isoform dependent and stimulus dependent. *American journal of physiology: Cell physiology* 2008; 295(3)**:** C768-C778.

33. Stark K, Eckart A, Haidari S, Tirniceriu A, Lorenz M, von Brühl ML *et al.* Capillary and arteriolar pericytes attract innate leukocytes exiting through venules and 'instruct' them with pattern-recognition and motility programs. *Nature Immunology* 2013; 14(1)**:** 41-51.

34. Nehls V, Drenckhahn D. Heterogeneity of microvascular pericytes for smooth muscle type alpha-actin. *Journal of Cell Biology* 1991; 113**:** 147–154.

35. Kornfield TE, Newman EA. Regulation of blood flow in the retinal trilaminar vascular network. *Journal of Neuroscience* 2014; 34(34)**:** 11504-11513.

36. Sims DE. Diversity Within Pericytes. *Clinical and Experimental Pharmacology and Physiology* 2000; 27(10)**:** 842–846.

37. Daneman R, Zhou L, Kebede AA, Barres BA. Pericytes are required for blood-brain barrier integrity during embryogenesis. *Nature* 2010; 468(7323)**:** 562-566.

38. Armulik A, Genové G, Mäe M, Nisancioglu MH, Wallgard E, Niaudet C *et al.* Pericytes regulate the blood-brain barrier. *Nature* 2010; 468(7323)**:** 557-61.

39. Reyahi A, Nik AM, Ghiami M, Gritli-Linde A, Pontén F, Johansson BR *et al.* Foxf2 Is Required for Brain Pericyte Differentiation and Development and Maintenance of the Blood-Brain Barrier. *Developmental Cell* 2015; 34(1)**:** 19-32.

40. Underly RG, Levy M, Hartmann DA, Grant RI, Watson AN, Shih AY. Pericytes as inducers of rapid, matrix metalloproteinase-9 dependent capillary damage during ischemia. *Journal of Neuroscience* 2016; in press.

41. Sagare AP, Bell RD, Zhao Z, Ma Q, Winkler EA, Ramanathan A *et al.* Pericyte loss influences Alzheimer-like neurodegeneration in mice. *Nature Communications* 2013; 4**:** 2932.

42. Hellström M, Kalén M, Lindahl P, Abramsson A, Betsholtz C. Role of PDGF-B and PDGFR-beta in recruitment of vascular smooth muscle cells and pericytes during embryonic blood vessel formation in the mouse. *Development* 1999; 126(14)**:** 3047-3055.

43. He L, Vanlandewijck M, Raschperger E, Andaloussi Mäe M, Jung B, Lebouvier T *et al.* Analysis of the brain mural cell transcriptome. *Science Reports* 2016; 6**:** 35108.

44. Zeisel A, Muñoz-Manchado AB, Codeluppi S, Lönnerberg P, La Manno G, Juréus A *et al.* Cell types in the mouse cortex and hippocampus revealed by single-cell RNA-seq. *Science* 2015; 6226(1138-1142).

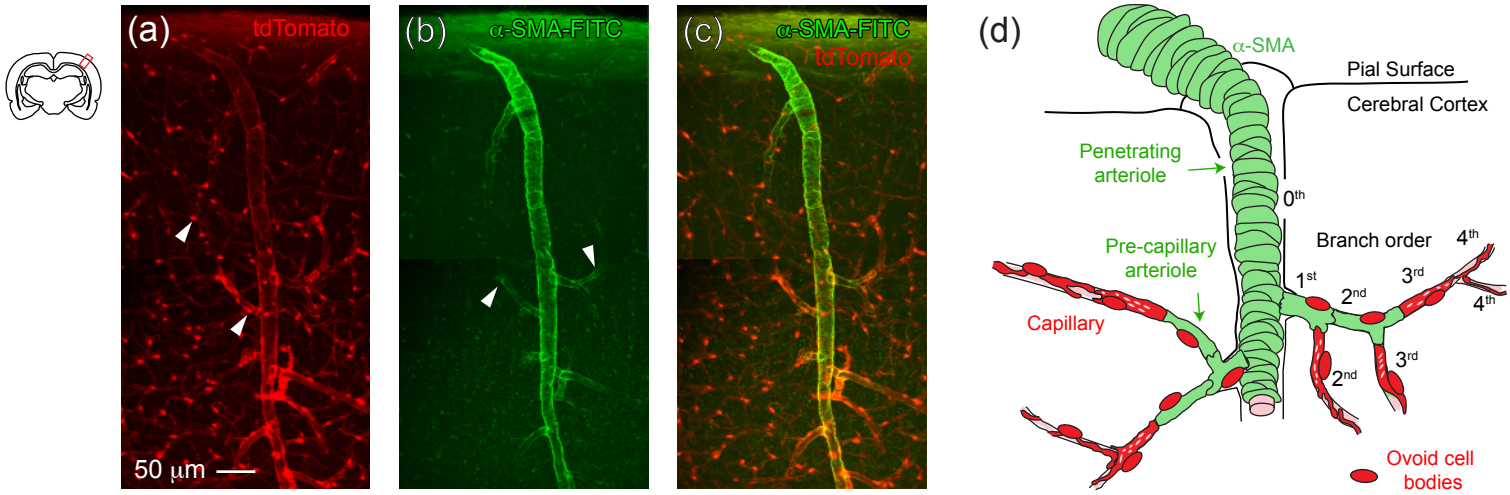

Figure 1 (Grant *et al.*)

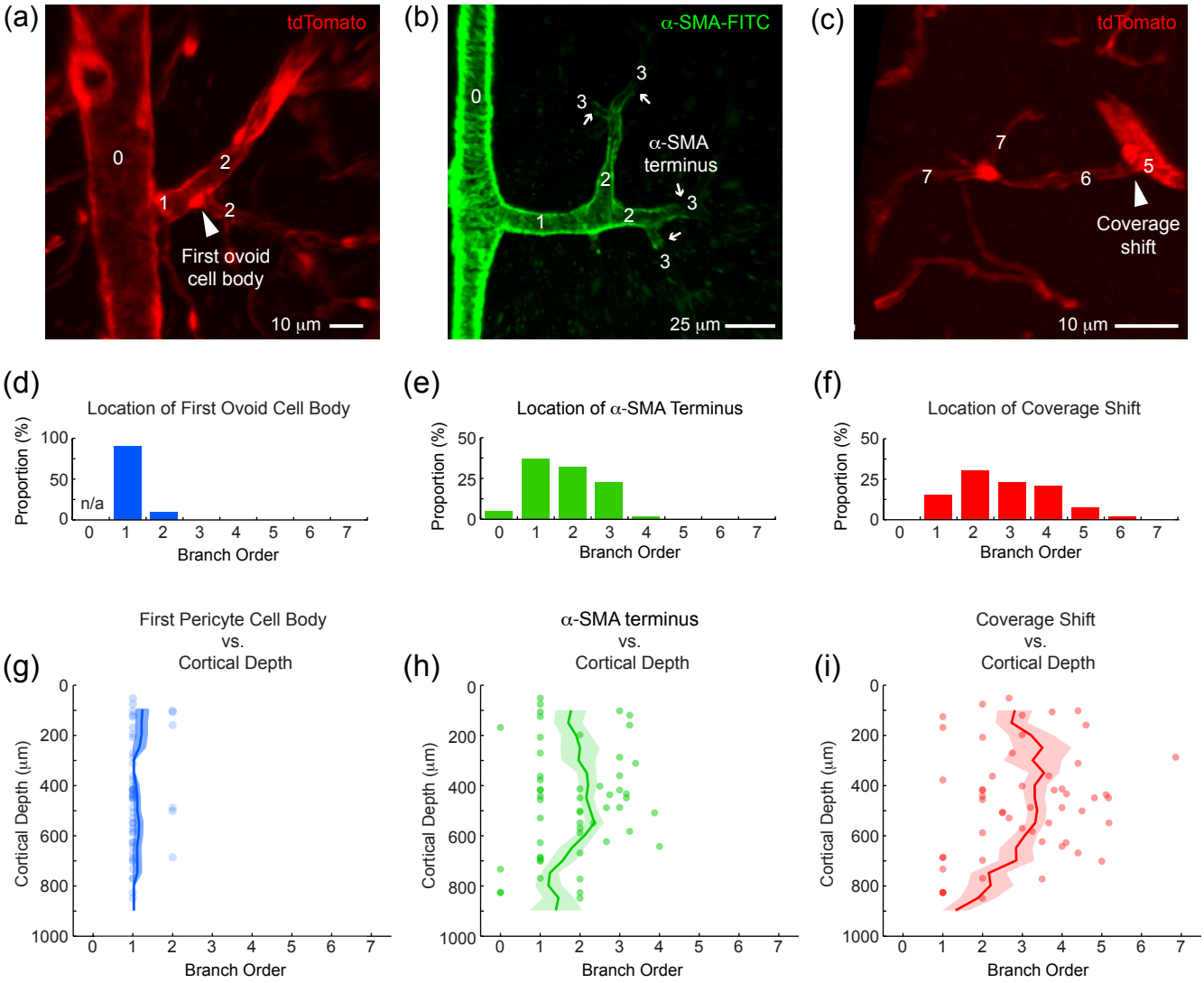

Figure 2 (Grant *et al.*)

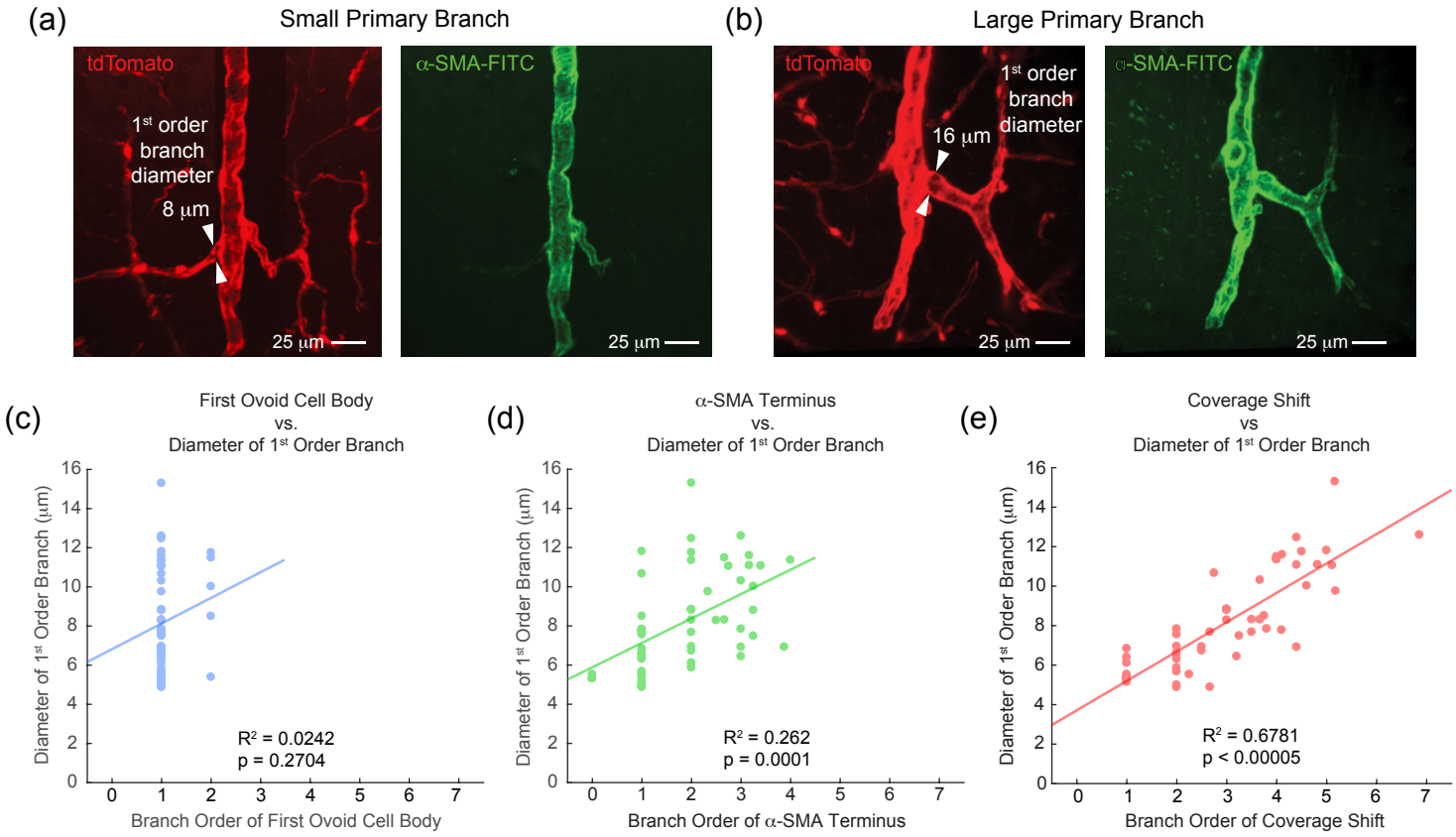

Figure 3 (Grant *et al.*)

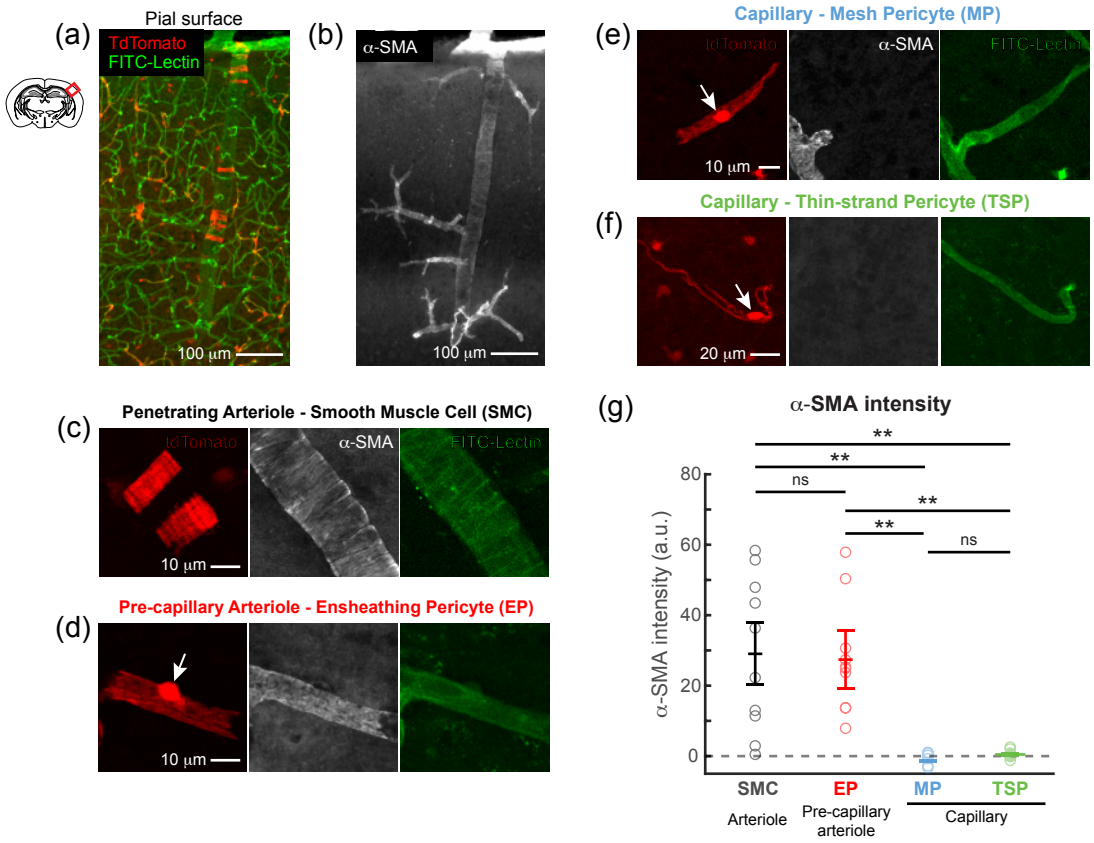

Figure 4 (Grant *et al.*)

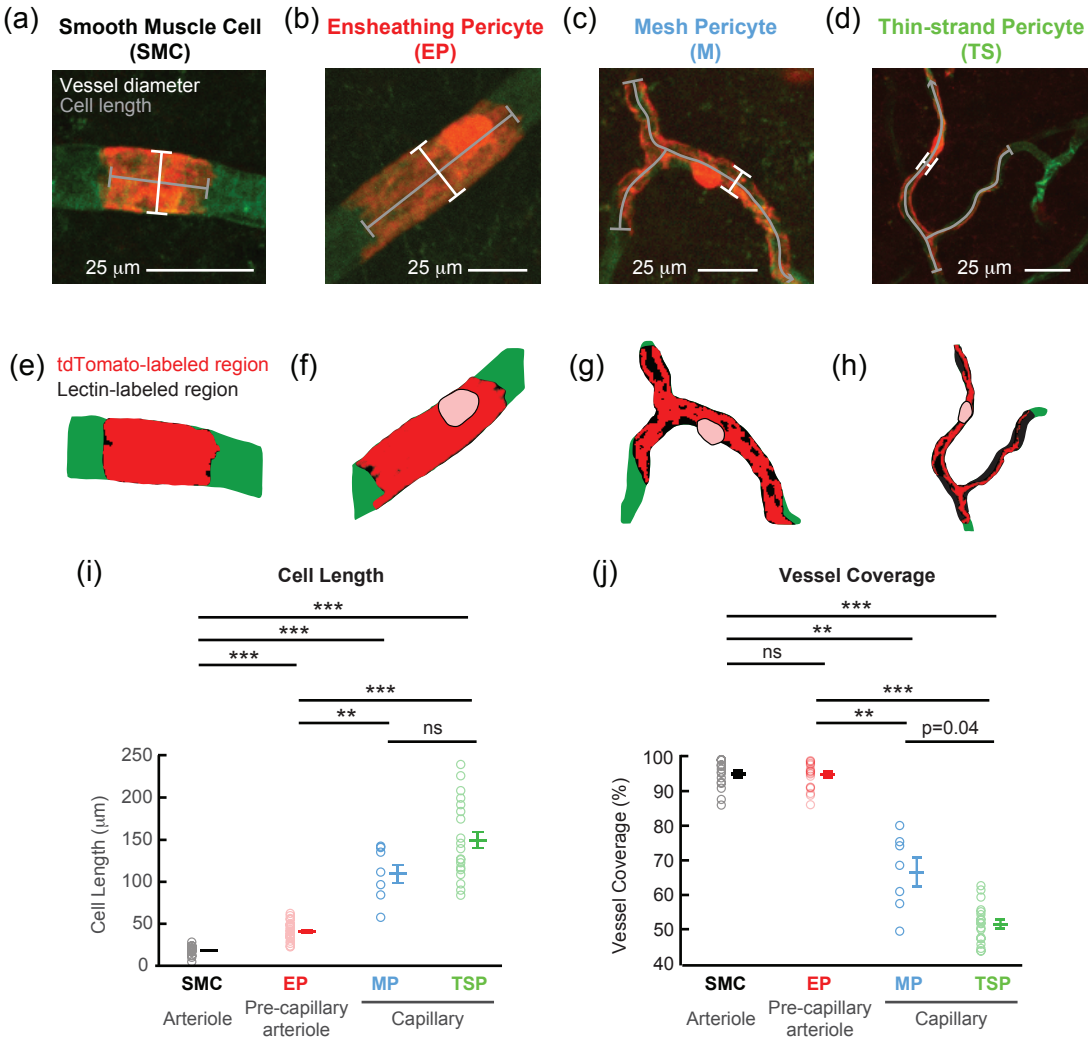

Figure 5 (Grant *et al.*)

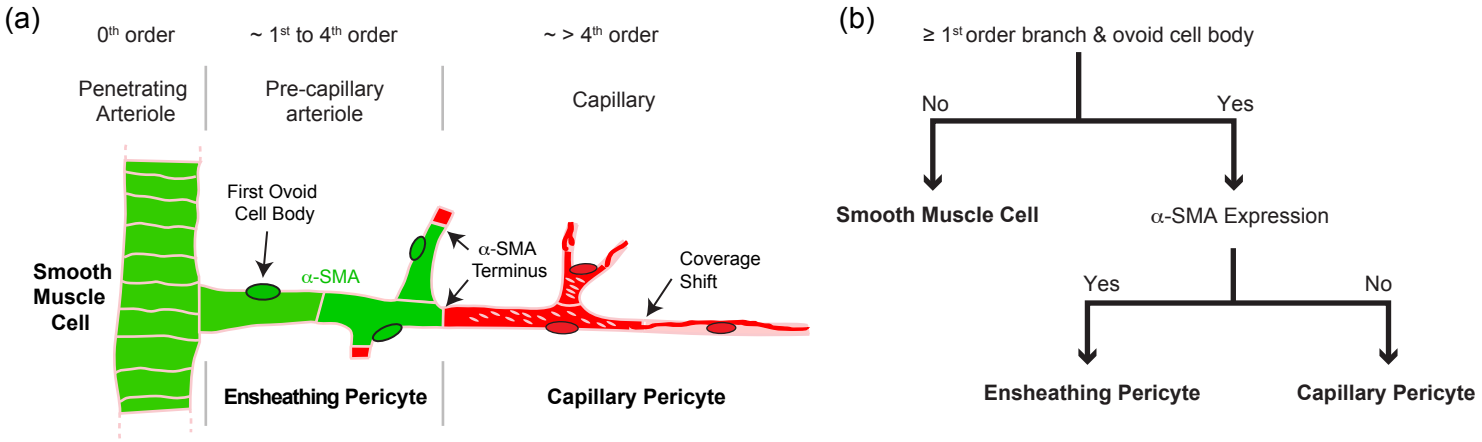

Figure 6 (Grant *et al.*)